Journal of Membrane Science 593 (2020) 117439

Contents lists available at ScienceDirect

Journal of Membrane Science

journal homepage: www.elsevier.com/locate/memsci

Theoretical modeling of the mass transfer performance of CO_2 absorption into DEAB solution in hollow fiber membrane contactor

Fan Cao, Hongxia Gao**, Hao Ling, Yangqiang Huang, Zhiwu Liang*

Joint International Center for CO_2 Capture and Storage (iCCS), Provincial Hunan Key Laboratory for Cost-effective Utilization of Fossil Fuel Aimed at Reducing Carbon-dioxide Emissions, College of Chemistry and Chemical Engineering, Hunan University, Changsha, 410082, PR China

ARTICLE INFO

Keywords:
Carbon dioxide
Hollow fiber membrane contactor
PTFE
DEAB
Mathematical modeling

ABSTRACT

4-diethylamino-2-butanol (DEAB), as a novel tertiary amine, shows a promising potential for CO_2 capture. In this study, the mass transfer performance of CO_2 absorption into aqueous DEAB solution in a non-wetted and partially-wetted mode of hollow fiber membrane contactor (HFMC) was theoretically investigated in comparison with that of monoethanolamine (MEA), diethanolamine (DEA), methyldiethanolamine (MDEA) and 2-amino-2-methyl-1-propanol (AMP). A 2D mathematical model based on finite element method (FEM) was established to solve the steady-state continuity equations for the shell, tube and membrane sides simultaneously. The influences of the operating parameters on the CO_2 absorption flux in HFMC including liquid and gas velocity and CO_2 partial pressure were comprehensively investigated. The numerical results show that the CO_2 absorption flux can increase with the increasing liquid velocity and CO_2 partial pressure, and slightly increases with the increasing gas velocity. Moreover, the CO_2 absorption performance of aqueous DEAB solution was further compared with different amine solutions, which reveals that the CO_2 absorption flux of DEAB is higher than those of DEA, MDEA and AMP, and is also comparable to MEA. The analysis on the mass transfer resistance indicates that the proportion of the membrane mass transfer resistance increased rapidly from 13.7% to 75.3% as membrane wetting ratio increased from 0% to 20%. Instead of the liquid phase, the mass transfer in wetted membrane phase becomes the rate-controlling step ultimately. The increase in the membrane wetting leads to the significant decrease in CO_2 absorption performance with 49.4% and 80.5% decrease in CO_2 absorption flux and the overall mass transfer coefficient at membrane wetting ratio of 5% and 50%, respectively. Based on the analysis on enhancement factor, it demonstrates that the chemical reaction between CO_2 and DEAB for the non-wetted mode generally occurs in the intermediate fast-instantaneous regime and gradually transfers to the instantaneous regime with membrane wetting.

1. Introduction

It is well known that the rapid growth of CO_2 emission is necessarily responsible for global warming as one of the major greenhouse gases. A variety of methods for capturing CO_2 have been proposed to mitigate the CO_2 emission from combustion of fossil-fuels, especially the flue gases of coal-fired power plants. Among these options for capturing CO_2, post-combustion CO_2 capture (PCCC) based on the chemical absorption technology has been considered to be one of the most developed commercial methods for removal of CO_2 from flue gas with low CO_2 partial pressure [1,2].

Typically, the packed columns are widely employed as the gas-liquid contactors to perform this CO_2 absorption process with amine-scrubbing strategies. Nevertheless, these conventional gas-liquid contacting equipments will inevitably encounter various operating problems such as foaming, flooding, channeling, entrainment, difficult calculation of gas-liquid mass transfer area and consequently, restrict industrial applications. Recently, the emerging membrane gas separation technology becomes one of the promising options which can eliminate the operational disadvantages based on the combination of the traditional gas absorption techniques and the novel membrane separation processes [3]+. The key concept of microporous membrane contactors is that they are employed as the non-selective physical barrier to allow non-dispersive contact between gas and liquid phases, which makes it possible to manipulate gas and liquid flow rates independently. Thus, the underlying flooding and entrainment frequently occurring in the conventional columns can be avoided in operation eventually. Moreover, the application of membrane contactors shows

* Corresponding author.
** Corresponding author.
E-mail addresses: hxgao@hnu.edu.cn (H. Gao), zwliang@hnu.edu.cn (Z. Liang).

https://doi.org/10.1016/j.memsci.2019.117439
Received 10 April 2019; Received in revised form 28 August 2019; Accepted 1 September 2019
Available online 01 September 2019
0376-7388/

more flexible operation in scaling up or down with much larger and well-defined mass transfer area in smaller equipment size due to the compact structure and modularity, leading to an enhancement of mass transfer rate. Also, the lower operational cost can be considered as one of the advantages superior to other conventional contactors [4,5].

Moreover, the process intensification of CO_2 mass transfer can be realized through membrane contactor coupled by the absorbents further. Therefore, it is very essential to choose appropriate and effective absorbents intended to be applied in the membrane contactors. So far, single and blended amines are regarded as the most widely used chemical absorbents for reducing CO_2 emission in conventional columns considering its extremely high CO_2 removal efficiency. In recent years, the amine-based absorbents have been gradually introduced and implemented in membrane contactor by many investigators. Monoethanolamine (MEA), as a typical primary amine, is the most developed and the benchmark amine for CO_2 capture due to its high CO_2 absorption rate [6,7]. However, its inherited disadvantages such as low CO_2 absorption capacity, high energy penalty for regeneration caused by carbamate formation, become the major limitations in the potential application. Similar drawbacks can be encountered in the use of the secondary amine such as Diethanolamine (DEA). As for a tertiary amine, e.g. N-methyldiethanolamine (MDEA), can generate bicarbonates only, resulting in a higher CO_2 absorption capacity than those of MEA and DEA, but much less reactive with CO_2 compared to MEA and DEA [8,9]. As a consequence, many efforts are made to investigate desirable amines with good CO_2 absorption-desorption performance such as faster CO_2 absorption rate, higher CO_2 absorption capacity, high mass transfer performance, lower regeneration energy consumption. Hence, one of the applicable and effective methods is to design and synthesize new amines or alkanolamines that can centralize the superiorities of different types of amines in a molecule [10,11]. In recent studies, some novel alkanolamines have been synthesized successfully based on a systematic structural modification of alkanolamines by a suitable placement of the substituents, particularly, where the relative position relationships between the hydroxyl group and amino group can affect CO_2 capture performance significantly. The best one of novel developed alkanolamines absorbents is 4-diethylamino-2-butanol (DEAB) by evaluation of the CO_2 absorption capacity and CO_2 cyclic capacity, as a tertiary amine, which was first synthesized in the International Test Centre for CO_2 Capture (ITC) [12,13]. It is found that the CO_2 absorption capacity of DEAB is higher than those of MEA, DEA, AMP and MDEA, but it can be competitive with PZ. Also, DEAB shows a better desorption performance due to lower regeneration energy consumption than those of MEA, DEA and MDEA [14,15]. Although, DEAB may be a good alternative absorbent based on excellent CO_2 absorption-desorption performance, it still remains a lab-scale application due to its complicated synthesis and poor economic effectiveness, which leads to immaturity in implementing comprehensive experimental investigation using membrane contactors. Thus, developing mathematical models can be accepted as one of the most effective and time-saving approaches to evaluate the mass transfer performance of CO_2 absorption into aqueous DEAB solution using hollow fiber membrane contactors. Currently, limited numerical investigations were performed based on a simplified model established under a non-wetted mode of operation to predict CO_2 concentration profile, CO_2 absorption flux and removal efficiency [16–18]. Nevertheless, the improved mathematical models which takes into consideration the effect of membrane wetting could be conducive to elucidating the accurate behavior of CO_2 mass transfer in membrane contactor, producing more reliable results [19–21].

The main propose of this work is to develop a 2D steady-state model for the theoretical investigation of mass transfer performance for CO_2 absorption into aqueous DEAB solution as a new amine absorbent under both non-wetted and partially-wetted modes of operation using a hollow fiber membrane contactor. A set of partial differential equations corresponding to mass transfer were solved by COMSOL Multiphysics software based on finite element method (FEM). The simulated CO_2 absorption flux of DEAB was used to compared with that of MEA, DEA, MDEA and AMP. Also, the effects of important operating parameters such as liquid and gas velocities, CO_2 partial pressure, amine concentration and liquid feed temperature on the CO_2 absorption performance, mass transfer resistance and the enhancement factor under the non-wetted and partially-wetted modes of operation were investigated.

2. Theory

2.1. Reaction kinetics of CO_2-amine-H_2O system

Generally, the reaction mechanism of amine with CO_2 is determined by the types and molecular structures of amines. As a well-established mechanism, the zwitterionic mechanism initially proposed by Caplow [22] and then reintroduced by Danckwerts [23] can be used to analyze the reaction between CO_2 and primary or secondary amines (i.e. MEA and DEA in this study) as the following reactions (1)–(6). In this mechanism, With CO_2 absorbed into primary or secondary amine, the first amine molecule reacts with CO_2 to form a zwitterion and finally forms a carbamate with the second amine molecule by deprotonation of the zwitterion.

$$H_2O \leftrightarrow H^+ + OH^- \tag{1}$$

$$CO_2 + H_2O \leftrightarrow H^+ + HCO_3^- \tag{2}$$

$$CO_2 + OH^- \leftrightarrow HCO_3^- \tag{3}$$

$$HCO_3^- \leftrightarrow H^+ + CO_3^{2-} \tag{4}$$

$$CO_2 + R_1NH_2 \leftrightarrow R_1NH_2^+COO^- \tag{5}$$

$$R_1NH_2^+COO^- + R_1NH_2 \leftrightarrow R_1NH_3^+ + R_1NCOO^- \tag{6}$$

$$R_1NHCOO^- + H_2O \leftrightarrow R_1NH_2 + HCO_3^- \tag{7}$$

For the MEA and DEA, the contribution of the reaction between CO_2 and H_2O (Eq. (2)) can be negligible to the overall reaction rate due to the extremely slow chemical reaction rate of CO_2 with H_2O. Moreover, the effect of OH^- on the overall reaction can be also negligible (Eq. (3)). Therefore, the reaction rate of MEA/DEA with CO_2 can be obtained by a second order reaction rate expression [24].

$$r_{CO_2} = k_{2,\text{amine1}}[\text{amine1}][CO_2] \tag{8}$$

where r_{CO2} is the overall reaction rate; $k_{2,amine1}$ is second order reaction constant of MEA and DEA; [amine1] and [CO_2] represent the concentration of MEA or DEA and the concentration of CO_2, respectively.

Nevertheless, the reaction between CO_2 and tertiary amine (i.e. DEAB and MDEA in this study) complies with base-catalyzed mechanism. Instead of direct reaction with CO_2, tertiary amine acts as a base catalyst for hydration of CO_2 as described in reactions (9)–(10) [25]. Moreover, compared to traditional primary or secondary amines, AMP is a sterically hindered primary alkanolamine with formation of bicarbonate due to the instability of the hindered amine carbamate, which is similar to reaction of CO_2 with tertiary amine as described in reaction (11) [26].

$$R_1R_2R_3N + H^+ \leftrightarrow R_1R_2R_3NH^+ \tag{9}$$

$$CO_2 + H_2O + R_1R_2R_3N \leftrightarrow R_1R_2R_3NH^+ + HCO_3^- \tag{10}$$

$$CO_2 + H_2O + AMP \leftrightarrow AMPH^+ + HCO_3^- \tag{11}$$

With regard to the effects of H_2O and OH^- on the overall reaction rate, the interactions of DEAB, MDEA and AMP with CO_2 can be regarded as second order reactions and further determined by the following equation.

$$r_{CO_2} = k_{2,\text{amine2}}[\text{amine2}][CO_2] \tag{12}$$

where $k_{2,amine2}$ is second order reaction constant of DEAB, MDEA and

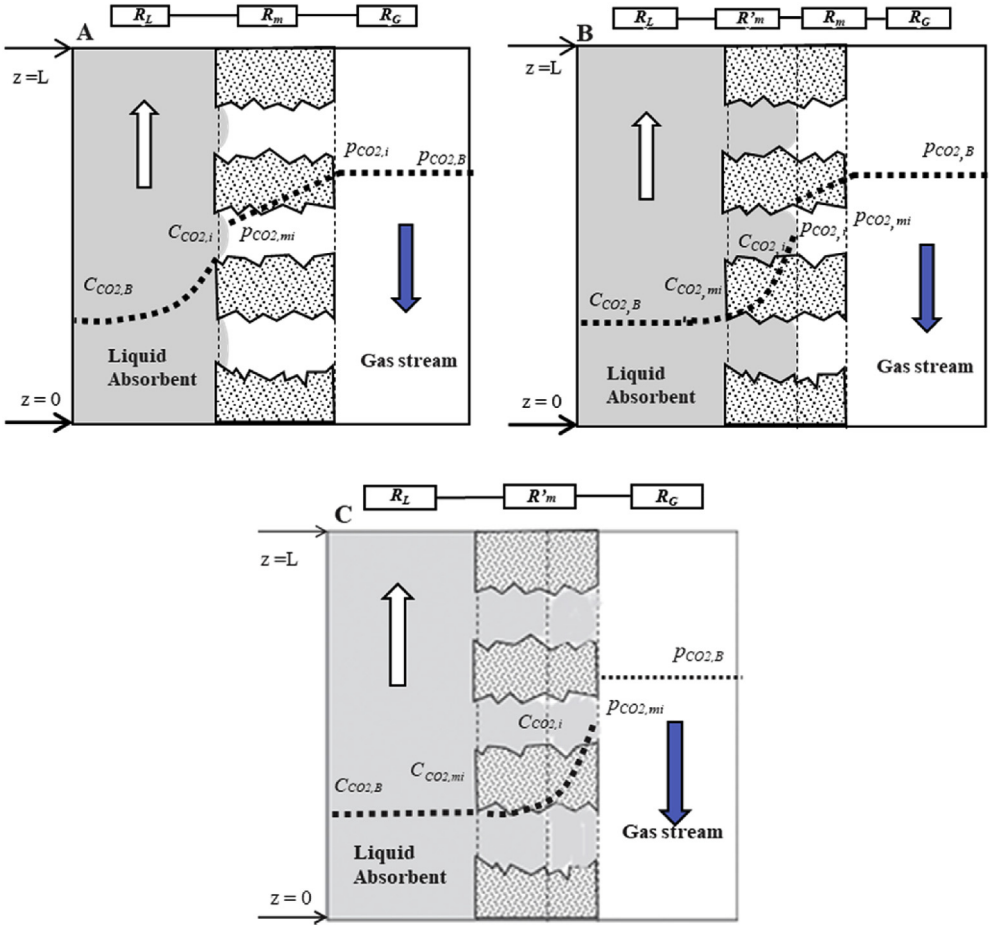

Fig. 1. The schematic diagram of mass transfer resistance-in series model under non-wetted mode of operation (A), partially-wetted mode of operation (B) and completely-wetted mode of operation (C).

AMP; [amine2] denote the concentration of DEAB, MDEA or AMP.

2.2. Mass transfer resistance in series model

The operation of gas-liquid membrane contactors can be classified into 3 modes including non-wetted (dry) mode, partially wetted mode, and wetted mode. In most cases of membrane CO_2 absorption process, the membrane contactors are generally operated in three modes, which include non-wetted, partially-wetted and completely-wetted modes as demonstrated in Fig. 1. The resistance in a series of models in the hollow fiber membrane module can be written as the following Eqs. (13)–(15) :

Non-wetted mode:

$$\frac{1}{K_G} = \frac{1}{EHk_L^o} + \frac{d_i}{k_m d_{ln}} + \frac{d_i}{k_G d_o} \tag{13}$$

Partially-wetted mode:

$$\frac{1}{K_G} = \frac{d_{\text{int}}}{EHk_L^o d_i} + \frac{d_{\text{int}}}{k_M d_{\text{ln}}} + \frac{d_{\text{int}}}{EHk'_m d'_{\text{ln}}} + \frac{d_{\text{int}}}{k_G d_o} \tag{14}$$

Completely-wetted mode:

$$\frac{1}{K_G} = \frac{1}{EHk_L^o} + \frac{Hd_i}{k'_m d'_{\text{ln}}} + \frac{d_i}{k_G d_o} \tag{15}$$

where K_G is the overall gas-phase mass transfer coefficient (m/s); k_G, k_m, $k'_m$and k_L^o are the individual mass transfer coefficients of the gas phase, the gas-filled membrane, the liquid-filled membrane and the liquid phase based on physical absorption (m/s), respectively; d_i, d_o, d_{ln} $d'_{ln}$and d_{int}represents the inner, interfacial, outer and logarithmic mean diameters of the non-wetted and wetted portion of the membrane (m/s), respectively; H denotes the Henry's constant (kmol/m^3 atm); and E is the enhancement factor.

Additionally, Eqs. (13)–(15) can be interpreted according to mass transfer resistance as presented in Eqs (16)–(18) :

$$R_{tot} = R_L + R_m + R_G \tag{16}$$

$$R_{tot} = R_L + R_m + R'_m + R_G \tag{17}$$

$$R_{tot} = R_L + R'_m + R_G \tag{18}$$

where $R_{tot}R_L$, R_m, R'_mandR_G represent the total mass transfer resistance, the mass transfer resistance of the liquid phase, the non-wetted membrane, the wetted membrane resistance, and the gas phase, respectively.

For the ideal non-wetted mode, the occurrence of mass transfer behavior is mainly divided into three stages: (1) the diffusion CO_2 molecules from the bulk gas to the membrane-gas interface; (2) the diffusion through membrane pores totally filled with gas to the liquid-membrane interface; and (3) the dissolution of CO_2 molecules into liquid absorbent. However, for the partially-wetted mode, the membrane pores are separated from two sections including liquid-filled portion and gas-filled portion, leading to more complicated situation for mass transfer in the membrane side. Many researchers have used the mass transfer resistance-in-series models to determine both the overall mass transfer resistance and individual resistance in each phase [27,28]. Moreover, the related equations are determined considering the fact liquid absorbent flows in the tube side while the gas stream flows in the shell side.

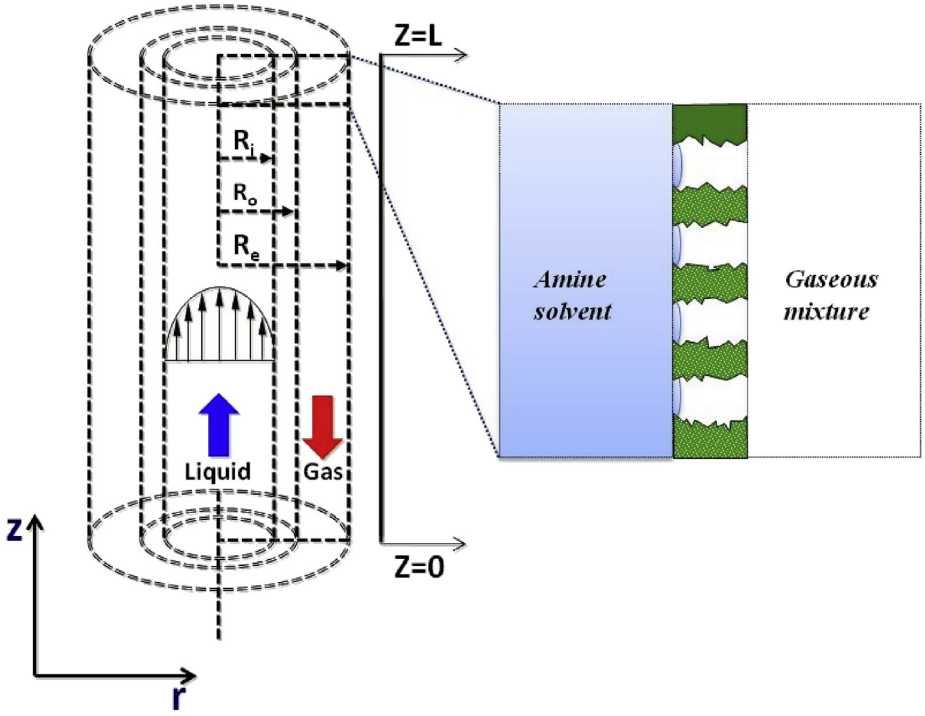

Fig. 2. The schematic diagram of CO_2 absorption in the PTFE hollow fiber membrane contactor.

2.3. Development of mathematical model

Fig. 2 exhibits a schematic diagram to interpret the process of the CO_2 reactive absorption into aqueous amine solution using a microporous PTFE HFMC. A single hollow fiber consists of three mass transfer domains, i.e. the tube side (liquid phase), the membrane side and the shell side (gas phase). As shown in Fig. 2, the liquid absorbent flows through the tube side while the gas stream is fed into the shell side counter-currently. A steady-state 2D mathematical axisymmetric model can be derived based on the following assumptions:

(1) The membrane gas absorption system remains isothermal conditions and steady-state;
(2) The liquid absorbent in the tube side presents a fully developed laminar parabolic distribution;
(3) Uniform properties of membrane are considered;
(4) Henry's Law is applicable for the gas-liquid equilibrium in the gas-liquid interface;
(5) Ideal gas behavior in the shell side of membrane contactor.

Based on the aforementioned assumptions, a series of steady-state continuity equations in all three domains are derived as follows:

2.3.1. Mass transfer in the tube side

The transportation of species in the tube side accounts for simultaneous chemical reaction, diffusion, and convection, hence, the steady-state continuity equation can be expressed as below:

$$V_{z-t}\frac{\partial C_{i-t}}{\partial z} = D_{i-t}\left(\frac{\partial^2 C_{i-t}}{\partial r^2} + \frac{1}{r}\frac{\partial C_{i-t}}{\partial r} + \frac{\partial^2 C_{i-t}}{\partial z^2}\right) + \nu_{i-t} \tag{19}$$

where D_{i-t}, C_{i-t} and ν_{i-t} are defined as the diffusion coefficient (m^2/s), concentration (mol/L), and chemical reaction rate (mol/s) for each species in the tube side, respectively; V_{z-t}denotes the tube axial liquid velocity; z and r represent the axial and radial coordinates, respectively. The liquid velocity profile in the tube side of hollow fiber membrane contactor is assumed to conform to Newtonian laminar flow as below [29].

$$V_{i-z} = 2\overline{V_t}\left(1 - \left(\frac{r}{r_i}\right)^2\right) \tag{20}$$

where $\overline{V_t}$ and r_i denote the average axial velocity of liquid in the tube region (m/s) and the inner radius of membrane fiber (m), respectively.

As liquid fluid flows through the tube side, the mass transfer coefficient of liquid phase can be determined via the well-known Graetz-Leveque mass transfer correlation proposed by Yang and Cussler [30].

For Gz (Graetz number) > 20

$$Sh = \frac{k_l^0 d_i}{D_{CO_2,L}} = 1.62\left(\frac{d_i}{L}ReSc\right)^{1/3} = 1.62G_Z^{1/3} = 1.62\left(\frac{v_l d_i^2}{D_{CO_2,L}L}\right)^{1/3} \tag{21}$$

where Sh, $Re$and $Sc$are the Sherwood number, Reynolds number and Schmidt number, respectively; $D_{CO_2,L}$ is the diffusion coefficient in the liquid absorbent (m^2/s); L is membrane fiber length (m); and v_l is the liquid velocity (m/s).

2.3.2. Mass transfer in the membrane side

2.3.2.1. Non-wetted mode of operation. In this mode of operation, there is no chemical reaction and convective mass transfer in the completely gas-filled membrane pores and overall mass transfer rate depends on diffusion. Therefore, the steady-state continuity equation in the membrane side can be rendered as the follows:

$$D_{CO_2-m}\left(\frac{\partial^2 C_{CO_2-m}}{\partial r^2} + \frac{1}{r}\frac{\partial C_{CO_2-m}}{\partial r} + \frac{\partial^2 C_{CO_2-m}}{\partial z^2}\right) = 0 \tag{22}$$

whereD_{CO_2-m}represents the diffusion coefficient of CO_2 in the membrane side, which is related to membrane pore size and the mean free path of CO_2, and can be calculated by the following equation.

$$\overline{\lambda} = \frac{3.2\mu}{P}\left(\frac{RT}{2M\pi}\right)^{0.4} \tag{23}$$

where $\overline{\lambda}$ is the mean free path of CO_2 (m); μ is dynamic viscosity (Pa·s); P is the gas pressure (Pa); R is ideal gas constant (8.314 J/mol·K); and M is the molar mass of gas (g/mol).

In this study, $0.01 < \overline{\lambda}/d_p < 0.1$, it indicates that CO_2 diffusion in the membrane pores is controlled by both molecular diffusion and Knudsen

diffusion.

Hence, the diffusion coefficient of CO_2 in the membrane side can be calculated based on the combination of molecular and Knudsen diffusivities as follows:

$$\frac{1}{D_{CO_2-m}} = \frac{1}{D_M} + \frac{1}{D_{Kn}} \tag{24}$$

where D_M and D_{Kn} represent the molecular and Knudsen diffusion coefficients (m^2/s), respectively.

The molecular self-diffusion coefficient of CO_2 can be determined based on the kinetic gas theory [31]:

$$D_M = 1200\frac{RT}{MP}\frac{\Omega_\mu}{\Omega_D}\mu \tag{25}$$

where R denotes the ideal gas constant, M represents the molecular weight of the gas; μ represents the dynamic viscosity of the gas; P represents the gas pressure (kPa). Ω_u and Ω_D demote the viscosity collision integral and diffusion collision integral, respectively.

$$\Omega_D = \frac{1.6036}{(\overline{T})^{0.1561}} + \frac{0.193}{\exp^{(0.47635\overline{T})}} + \frac{1.033587}{\exp^{(1.52996\overline{T})}} + \frac{1.76474}{\exp^{(3.89411\overline{T})}} \tag{26}$$

$$\Omega_\mu = \frac{1.16145}{(\overline{T})^{0.14675}} + \frac{0.52487}{\exp^{(0.7732\overline{T})}} + \frac{2.16178}{\exp^{(2.43787\overline{T})}} \tag{27}$$

$\overline{T}$ denotes dimensionless temperature: $\overline{T} = \kappa T/\varepsilon$, where κ and ε are the Boltzmann constant and the parameter of the Stockmayer potential, respectively which can be calculated according to the critical temperature [32].

The Knudsen diffusion coefficient can be determined as follows [33]:

$$D_k = 48.5 d_o \sqrt{\frac{T_G}{M}} \tag{28}$$

where T_G is the gas temperature, and d_o is the mean pore diameter of membrane.

For the completely gas-filled membrane pores, i.e., non-wetted mode of operation, the mass transfer coefficients of the membrane can be determined from the following equation:

$$k_m = \frac{D_{CO_2-m}\varepsilon_m}{\tau_m \delta_{non-wetted}} \tag{29}$$

where ε_m and τ_m are the porosity, tortuosity of the membrane, respectively; and $\delta_{non-wetted}$ is the thickness of the gas-filled membrane pores (non-wetted membrane).

2.3.2.2. Partially-wetted mode of operation. The Partially-wetted membrane pores are divided into two regions, i.e., liquid-filled region and gas-filled region as shown in Fig. 3.

For the partially-wetted mode of operation, the wetting ratio (X_{wetted}) can be regarded as the evaluation of extent of membrane wetting:

$$X_{wetted} = \frac{\delta_{wetted}}{r_o - r_i} \tag{30}$$

where δ_{wetted} is the thickness of the liquid-filled membrane pores (wetted membrane) (m).

By contrast, the transportation of species in the liquid-filled membrane pores involves the diffusion and chemical reactions. Hence, the related steady-state continuity equation can be derived as in Eq. (31):

$$D_{i-L-m}\left(\frac{\partial^2 C_{i-L-m}}{\partial r^2} + \frac{1}{r}\frac{\partial C_{i-L-m}}{\partial r} + \frac{\partial^2 C_{i-L-m}}{\partial z^2}\right) + \nu_{i-m} = 0 \tag{31}$$

Due to the porosity of hollow fiber membrane, the region where the chemical reactions actually take place in the membrane side is located within the liquid-filled membrane pores only. Hence, in this case, the real chemical reactions can be written as below [24,34]:

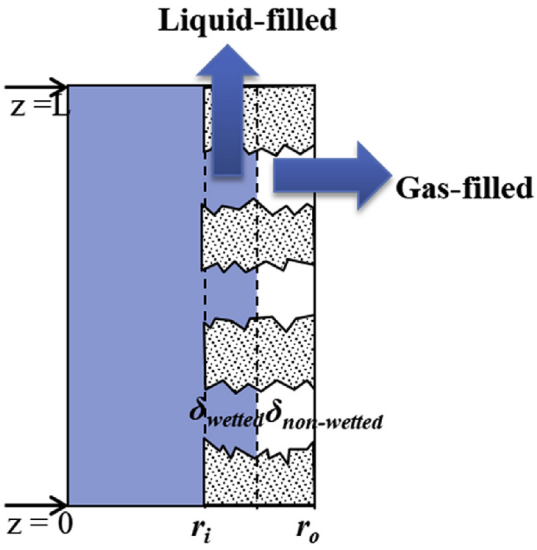

Fig. 3. A schematic diagram of partially-wetted of mode in the membrane fiber.

$$\nu_{i-m} = \nu_{i-t} \times \varepsilon_m \tag{32}$$

where D_{i-L-m} and ν_{i-m} are the diffusion coefficient for specie i (m^2/s) and the reaction rate for specie i within the liquid-filled portion in the membrane pores (mol/m^3 s), respectively.

For the gas-filled portion of membrane pores, the diffusion is only mechanism of mass transfer of CO_2. Therefore, the related steady-state continuity equation similar to that in case of non-wetted mode can be derived as:

$$D_{CO_2-G-m}\left(\frac{\partial^2 C_{CO_2-G-m}}{\partial r^2} + \frac{1}{r}\frac{\partial C_{CO_2-G-m}}{\partial r} + \frac{\partial^2 C_{CO_2-G-m}}{\partial z^2}\right) = 0 \tag{33}$$

where D_{CO_2-G-m} represents the diffusion coefficient of CO_2 within the gas-filled portion in the membrane pores, which is equal to D_{i-m} (m^2/s).

For the completely liquid-filled membrane pores, i.e., wetted mode of operation, the mass transfer coefficients of the membrane can be calculated from the following equation:

$$k_m' = \frac{D_{CO_2,L}\varepsilon_m}{\tau_m \delta_{wetted}} \tag{34}$$

In combination of the mass transfer coefficients of non-wetted and wetted membrane, the corresponding calculation of partially-wetted membrane can be formulated as below:

$$\frac{1}{k_m^p} = \frac{X_{wetted}}{k_m'} + \frac{1 - X_{wetted}}{k_m} \tag{35}$$

k_m^p is the mass transfer coefficient of partially-wetted membrane (m/s).

2.3.3. Mass transfer in the shell side

The gas stream flows through the shell side without chemical reactions. Thus, the mass transfer in the shell side just accounts for the effects of diffusion and convection. Accordingly, the steady-state continuity equations can be written as:

$$V_{z-s}\frac{\partial C_{CO_2-s}}{\partial z} = D_{CO_2-s}\left(\frac{\partial^2 C_{CO_2-s}}{\partial r^2} + \frac{1}{r}\frac{\partial C_{CO_2-s}}{\partial r} + \frac{\partial^2 C_{CO_2-s}}{\partial z^2}\right) \tag{36}$$

The velocity profile in the shell side can be described based on Happel's free surface model is applied [35]:

$$V_{z-s} = 2\overline{V}_{z-s}\left(1 - \left(\frac{r_o}{r_e}\right)^2\right) \times \left[\frac{(r/r_e)^2 - (r_o/r_e)^2 + 2In(r_o/r)}{(r_o/r_e)^4 - 4(r_o/r_e)^2 + 4In(r_o/r_e) + 3}\right] \tag{37}$$

where $\overline{V}_{z-s}$ is the average velocity in the shell side (m/s), r_e represents the free surface radius (m/s), which can be calculated by the following

expression:

$$r_e = r_o\sqrt{1/(1-\varphi)} \tag{38}$$

Where ϕ is interpreted as the void volume fraction of the hollow fiber membrane module and is determined by the following equation:

$$\varphi = 1 - n\frac{r_o^2}{r_i^2} \tag{39}$$

where n and R_i represent the number of membrane fibers and the inner module radius, respectively.

For the gas fluid in the shell side, the correlation of prediction for the mass transfer coefficient of gas phase can be described as follows [30]:

$$Sh = \frac{k_G d_e}{D_{CO_2,G}} = 1.25\left(\frac{d_e}{L}Re\right)^{0.93} Sc^{0.33} \tag{40}$$

Where $d_e$is the hydraulic diameter.$D_{CO_2,G}$ is the diffusion coefficient in the gas phase (m^2/s).

2.4. Enhancement factor

The enhancement factor (E) is an important parameter accounting for the effect of chemical reaction on mass transfer and can be defined as the ratio of absorption flux in the absence and presence of chemical reactions. It is a function of the Hatta number (Ha) and the infinite enhancement factor (E_∞). An approximate solution for estimation of enhancement factor was as the following equation proposed by DeCoursey [36]:

$$E = \frac{-Ha^2}{2(E_\infty - 1)} + \sqrt{\frac{Ha^4}{4(E_\infty - 1)^2} + \frac{E_\infty Ha^2}{(E_\infty - 1)} + 1} \tag{41}$$

The Hatter number (Ha) is the ratio of maximum reactive conversion to the maximum diffusion mass transfer as the following equation:

$$Ha = \frac{\sqrt{k_{2,a\,\min e} D_{CO_2,L} C_{a\,\min e}}}{k_{L,ext}} \tag{42}$$

where $k_{2,a\,\min e}$ represents the second-order reaction rate constant of CO_2-amine reaction (L/mol s), $C_{a\,\min e}$ is the concentration of amine (mol/L), and $k_{L,ext}$ is the total mass transfer coefficient of the liquid phase (m/s). The partially-wetted mode accounts for the liquid-filled membrane pores and it can be given by:

$$k_{L,ext} = \frac{k_L^0}{1 + (k_L^0/k_m')(d_i/d_{\ln}')} \tag{43}$$

while for a non-wetted mode, $k_{L,ext}$is equal to Ref. k_L^0[37].

Leveque's model can be used to calculate the infinite enhancement factor as follows:

$$E_\infty = \left(1 + \frac{C_{a\,\min e} D_{a\,\min e,L}}{\upsilon_{a\,\min e} C_{CO_2,i} D_{CO_2,L}}\right)\left(\frac{D_{CO_2,L}}{D_{a\,\min e,L}}\right)^{1/3} \tag{44}$$

where $D_{a\,\min e,L}$ is the diffusion coefficient of amine in solution (m/s), $\upsilon_{a\,\min e}$represents the stoichiometric coefficient of amine in the reaction and $C_{CO_2,i}$ is the concentration of CO_2 at the interface of the liquid phase (mol/L), which can be determined according to the following equation;

$$C_{CO_2,i} = \left(\frac{P_{CO_2,G} + (k_{L,ext}(d_i/d_o)E/k_{G,ext})C_{CO_2,B}}{1 + (k_{L,ext}(d_i/d_o)E/k_{G,ext})}\right)H \tag{45}$$

where $k_{G,ext}$represents the total mass transfer coefficient of the gas phase (m/s). Based on a combination of gas and membrane mass transfer coefficients, it can be given by the following expression:

$$k_{G,ext} = \frac{k_G/RT}{1 + (k_G/k_m)(d_i/d_{\ln})} \tag{46}$$

Henry's constant of CO_2 in amine solution can be determined based on the N_2O analogy:

$$H_{CO_2-a\,\min e} = H_{N_2O-a\,\min e}\left(\frac{H_{CO_2-H_2O}}{H_{N_2O-H_2O}}\right) \tag{47}$$

where $H_{N_2O-a\,\min e}$ represents Henry's constant of N_2O in aqueous amine; $H_{CO_2-H_2O}$and $H_{N_2O-H_2O}$ are Henry's constants of CO_2 and N_2O in water, respectively, which can be calculated by the following equation proposed by Versteeg and Swaalj [38].

$$H_{N_2O-H_2O} = 8.547 \times 10^6 \exp\left(-\frac{2284}{T/K}\right) \tag{48}$$

$$H_{CO_2-H_2O} = 2.8249 \times 10^6 \exp\left(-\frac{2044}{T/K}\right) \tag{49}$$

Moreover, the dimensionless Henry's constant (H_d) can be presented by:

$$H_d = \frac{RT}{H} \tag{50}$$

2.5. Numerical solution

A set of governing partial differential equations derived for the material balance in the tube, the membrane and the shell side with appropriate boundary conditions (as listed in Table 1) were solved based on finite elements method (FEM) by COMSOL Multiphysics software (Version 5.3a), which can divide different domains in the hollow fiber membrane contactor into small dimension units to obtain the simulated results of important parameters such as CO_2 concentration profiles at each point of the domains. The Specifications of membrane and the related physical and chemical parameters are listed in Table 2 and Table 3, respectively. An internal numerical solver of COMSOL, PARDISO, is employed to achieve self-adaptive meshing and

Table 1
The boundary conditions for the shell, tube and membrane sides.

Position	Tube side	Membrane side		Shell side
		Non-wetted	Partially-wetted	
z = 0 (liquid-inlet, gas-outlet) z = L (liquid-outlet, gas-inlet)	$C_{CO_2-t} = 0 C_{a\,\min e-t} = C_{a\,\min e-initial}$,			$C_{CO_2-s} = C_{CO_2-initial}$
$r = 0$	$\frac{\partial C_{i-t}}{\partial r} = 0 (i = CO_2, \text{amine})$			
$r = r_i$	$C_{CO_2-t} = m \times C_{CO_2-m}\frac{\partial C_{a\,\min e-t}}{\partial r} = 0$,	$C_{CO_2-m} = \frac{C_{CO_2-t}}{m}\frac{n!}{r!(n-r)!} C_{i-L-m} = C_{i-t}$		
$r = r_o$		$C_{CO_2-m} = C_{CO_2-s}$		$C_{CO_2-s} = C_{CO_2-G-m}$
$r = r_e$				$\frac{\partial C_{CO_2-s}}{\partial r} = 0$
$r = r_w$		$C_{CO_2-L-m} = C_{CO_2-G-m} \times m\frac{\partial C_{s-m}}{\partial r} = 0$		

Table 2
Specifications of the hollow fiber PTFE membrane and module.

Parameters	Value
Membrane module length. L (mm)	200*3
Membrane module i.d. r_m (mm)	18
Membrane number of fibers. (n_f)	20
Membrane Fiber O.D. r_o (mm)	1.7
Membrane Fiber I.D. r_i (mm)	1.0
Porosity, ε_m	0.5
Tortuosity, τ $\tau = (2-\varepsilon_m)^2/\varepsilon_m$	4.5
Membrane average pore size, r_{mp} (μm)	0.3

Table 3
Physicochemical Parameters of amine used for the model (T = 298 K, C_{amine} = 2 mol/L).

Paramater	Expression	literature
$k_{2,DEAB}$(m^3■mol^{-1}■s^{-1})	$4.01\times10^{13}\exp^{(-7527.7/T)}$	[39]
$k_{2,MEA}$ (m^3■mol^{-1}■s^{-1})	$5.127\times10^{13}\exp^{(-3373.8/T)}$	[40]
$k_{2,DEA}$(m^3■mol^{-1}■s^{-1})	$\exp^{(24.515-5411.3/T)}/1000$	[41]
$k_{2,AMP}$(m^3■mol^{-1}■s^{-1})	$\exp^{(17.2-3152/T)}/1000$	[26]
$k_{2,MDEA}$(m^3■mol^{-1}■s^{-1})	$1.34\times10^{6}\exp^{(-5771/T)}$	[25]
D_{CO_2-G-s}(m^2/s)	$\frac{(4.36\times10^{-5})T_G^{3/2}\sqrt{\frac{1}{M_A}+\frac{1}{M_B}}}{P(v_A^{1/3}+v_B^{1/3})}$	[42]
D_M(m^2/s)	9.294×10^{-6}–9.141×10^{-6}	[31]
D_K(m^2/s)	7.57×10^{-5}	[33]
$D_{CO_2,L}$for water (m^2/s)	$2.35\times10^{-6}\exp^{(-2119/T)}$	[38]
$D_{CO_2,L}$for DEAB (m^2/s)	1.12×10^{-9}	[13]
$D_{CO_2,L}$for MEA (m^2/s)	1.60×10^{-9}	[43]
$D_{CO_2,L}$for DEA (m^2/s)	9.05×10^{-10}	[43]
$D_{CO_2,L}$for AMP (m^2/s)	7.87×10^{-10}	[43]
$D_{CO_2,L}$for MDEA (m^2/s)	1.11×10^{-9}	[43]
$D_{DEAB,L}$(m^2/s)	3.82×10^{-10}	[44]
$D_{MEA,L}$(m^2/s)	9.19×10^{-10}	[45]
$D_{DEA,L}$(m^2/s)	5.4×10^{-10}	[45]
$D_{AMP,L}$(m^2/s)	7.87×10^{-10}	[46]
$D_{MDEA,L}$(m^2/s)	4.58×10^{-10}	[45]
$H_d = RT/H$for H_2O	$H = 8.2849\times10^{6}\exp^{(-2044/T)}$	[38]
$H_d = RT/H$for DEAB	0.856	[13]
$H_d = RT/H$for MEA	0.797	[47]
$H_d = RT/H$for DEA	0.710	[47]
$H_d = RT/H$for AMP	0.513	[47]
$H_d = RT/H$for MDEA	0.789	[47]

efficient error control in simulation, which is also an implicit time-stepping scheme and especially well-suitable for the solution of partial differential equations even in case of stiff non-linear boundary conditions. Here, a personal computer equipped with RAM 32.00 GB and Intel(R) Core (TM) i7 CPU 7700HQ @3.5 GHz and 64-bit operating system was used to solve the partial differential equations.

2.6. Determination of CO_2 absorption flux

CO_2 absorption flux (J_{CO_2}) represents the efficiency of CO_2 absorption with the calculation as below:

$$J_{CO_2} = \frac{G(Y_{in} - Y_{out})}{A_i} \tag{51}$$

where$G$is the gas flow rate (inlet kmol air/s); Y_{in} and Y_{out} are the molar ratios of CO_2 to air for inlet and outlet gas (kmol CO_2/kmol Air), respectively; and A_i denotes the total mass transfer area calculated based on the inner surface of the membrane.

3. Results and discussion

In this study, the mathematical model established by COMSOL software has been employed to investigate the effects of the operating parameters (i.e. liquid velocity, gas velocity, CO_2 partial pressure, liquid feed temperature and amine concentration) and membrane wetting behavior on the mass transfer performance of CO_2 absorption into aqueous DEAB solution using a hollow fiber membrane contactor. Additionally, the CO_2 concentration profiles along axial and radical directions in the membrane contactor were studied as well as the variation of the enhancement factor of the non-wetted and partially wetted with partial operational parameters. Also, the analysis of mass transfer resistance was made to provide the valuable insight into the behavior of CO_2 absorption in HFMC.

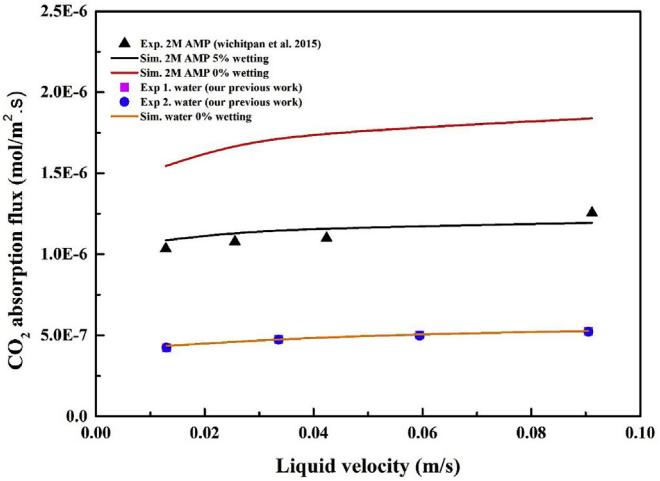

Fig. 4. Model validation for simulated CO_2 absorption flux compared with experimental results (Water, AMP 2 mol/L; CO_2 partial pressure 20 kPa; Gas velocity 0.239 m/s; Temperature 298 K.

3.1. Model validation

The application of a novel absorbent reveals that no related experimental data in the literature is available for CO_2 absorption in aqueous DEAB solution using hollow fiber membrane contactors. Accordingly, the correctness of the non-wetted and partially-wetted models were validated by the experimental results of CO_2 absorption into water from our previous work and 2 M aqueous AMP solution from the reported work of Rongwong et al. [48]. As presented in Fig. 4, the simulated results for the non-wetted case as a function of liquid velocity show the good agreement with the experimental results, thereby verifying the inexistence of membrane wetting using water as a physical absorbent. By contrast, the experimental results of AMP as chemical absorbent are significantly lower than the predicted results for the non-wetted case, but in much better agreement with the corresponding values considering 20% membrane wetting.

3.2. The comparison between DEAB and conventional amines for the CO_2 absorption flux

Liquid velocity is generally regarded as a key operational parameter that has a remarkable effect on the performance of a typical CO_2 absorption process. CO_2 absorption flux in a wide range of liquid velocity of 0.012 m/s-0.089 m/s for various amine-based solvents in non-wetted mode is plotted in Fig. 5. As shown in the Figure, the CO_2 absorption flux of DEAB solution increases with increasing liquid velocity. Similar observations have been widely reported that the increasing liquid velocity (i.e. higher turbulence in liquid flow) can lead to an enhancement in the mass transfer coefficient in HFMC with the increase in mass transfer coefficient of liquid phase (i.e. the decreased liquid resistance), according to Eqs (13) and (21). As a result, it gives rise to a decreased boundary layer thickness of the liquid phase and larger effective gas-

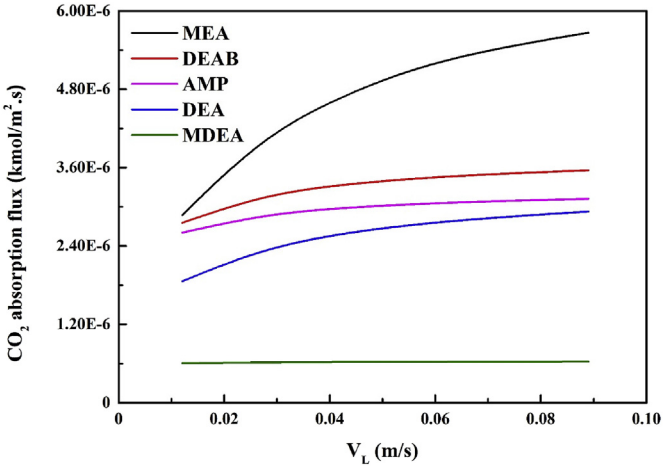

Fig. 5. The effect of liquid velocity on the CO_2 absorption flux (amine 2 mol/L; CO_2 partial pressure 20 kPa; Gas velocity 0.159 m/s; liquid feed temperature 298 K; CO_2 loading 0 mol/mol).

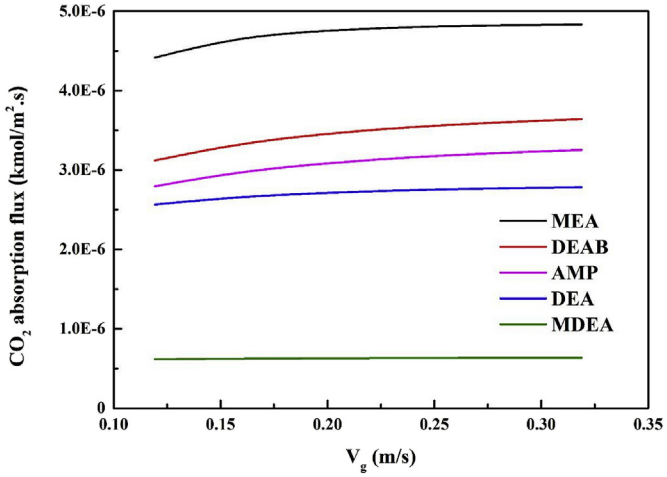

Fig. 6. The effect of gas velocity on the CO_2 absorption flux (amine 2 mol/L; CO_2 partial pressure 20 kPa; Liquid velocity 0.042 m/s; liquid feed temperature 298 K; CO_2 loading 0 mol/mol).

liquid contacting area, allowing more reactive amine molecules to spread to and react with CO_2 around the inner membrane surface. It can be also seen in Fig. 5, the enhancement in CO_2 absorption flux using DEAB solution is more significant at lower liquid velocities. i.e., CO_2 absorption flux increases by 21.3% as liquid velocity increases from 0.012 m/s to 0.042 m/s; while liquid velocity continues to increase to 0.089 m/s, the value of flux rises by 6.66% accordingly.

In addition, the residence time of amine solvents in the tube side becomes shorter with increasing liquid velocity associated with the absorbed CO_2 in the liquid phase shipped out of membrane contactor, resulting in a lower CO_2 concentration in the liquid phase and subsequently, higher CO_2 concentration gradient between gas and liquid phases. Consequently, the mass transfer rate is further intensified [19]. Also, the effect of liquid velocity on CO_2 absorption flux in different amine systems varied in the whole range. For MDEA, the visible growth of CO_2 absorption flux is hardly observed by increasing liquid velocity due to its very low reaction rate with CO_2. By contrast, MEA has the highest CO_2 absorption flux due to its much higher reaction rate than that of other amines. Although DEAB has a lower CO_2 absorption rate than that of DEA, its higher CO_2 absorption capacity leads to higher CO_2 absorption flux based on the fact that consuming 1 mol CO_2 just requires 1 mol DEAB. Moreover, it may be inferred that, compared to DEAB, the mass transfer performance of CO_2 absorption in aqueous AMP solution is largely limited by the less diffusion coefficient of CO_2 in AMP solution in spite of its higher CO_2 absorption rate.

The influence of gas velocity on CO_2 absorption flux was investigated for various amine-based solvents and non-wetted mode by increasing the gas velocity in the range from 0.119 m/s to 0.319 m/s. As illustrated in Fig. 6, the simulated results for different amine solvents reveals that increasing gas velocity has a promoting effect on the CO_2 absorption performance. This phenomenon can be explained by the fact that increasing flue gas velocity can enhance the mass transfer in the gas phase, and thus, enhance the mass transfer through the membrane. Also, DEAB is the most affected solvent by increasing the gas velocity at low gas velocities, because it has high absorption capacity and moderate reaction rate with CO_2. By contrast, MDEA has no significant variation in CO_2 flux by increasing the gas velocity due to its low reaction rate with CO_2 and the low CO_2 equilibrium solubility. Moreover, the CO_2 absorption flux of all amine solutions studied in this work becomes gradually constant at higher gas velocities, which is caused by the predominant contribution of liquid-phase and membrane resistance to the overall mass transfer resistance in this condition. The similar observation was reported by Masoumi et al. [17], Cui and Demontigny [49].

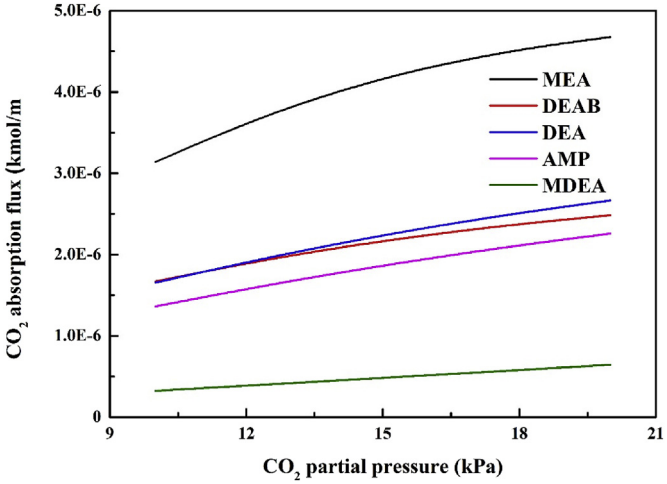

Fig. 7. The effect of CO_2 partial pressure on the CO_2 absorption flux (amine 2 mol/L; Liquid velocity 0.042 m/s; Gas velocity 0.159 m/s; liquid feed temperature 298 K; CO_2 loading 0 mol/mol).

The effect of CO_2 partial pressure on CO_2 absorption performance into different amine solution is investigated in the CO_2 partial pressure range of 10–20 kPa. As represented in Fig. 7, the values of CO_2 absorption flux increase as the CO_2 partial pressure increases. This phenomenon can be explained according to the fact below: the increasing CO_2 partial pressure can increase the concentration of CO_2 in the gas-mixture, and then more CO_2 molecules diffuse to the gas-liquid contacting interface from gas bulk through membrane pores, leading to a higher mass transfer driving force. Therefore, the higher CO_2 absorption flux is achieved. For instance, the CO_2 absorption flux in the DEAB enhances from 1.88E-6 to 3.34E-6 mol/m^2·s with increasing the CO_2 partial from 10 to 20 kPa. Moreover, as can be seen in this Fig. 7, at high CO_2 partial pressure, the growth in CO_2 absorption flux for secondary amines (DEA) decreases faster than those of tertiary and sterically hindered amine (DEAB and AMP). It can be explained by the higher absorption capacity of tertiary and sterically hindered amines compared to DEA.

The CO_2 concentration profiles along the axial direction through three regions including the shell side, membrane side, and liquid phase at the middle of the membrane contactor (1/2L) are demonstrated in Fig. 8. When the membrane suffers various degrees of membrane wetting, there is no significant reduction of CO_2 concentration in the shell

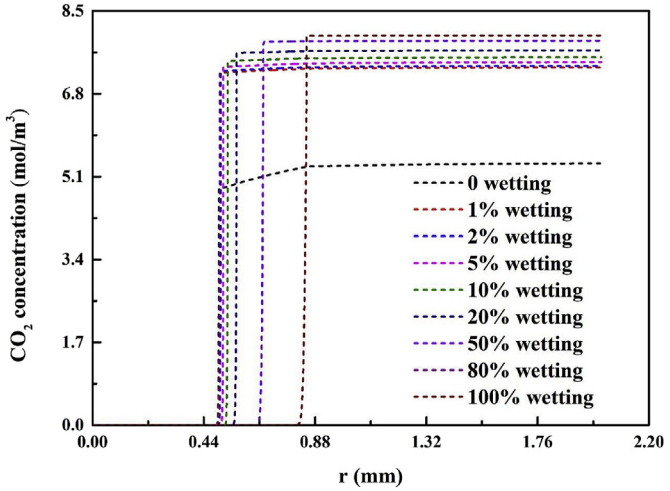

Fig. 8. The radical CO_2 Concentration at the middle of the membrane contactor (1/2*L*) (DEAB 2 mol/L; CO_2 partial pressure 20 kPa; CO_2 Liquid velocity 0.042 m/s; Gas velocity 0.159 m/s; liquid feed temperature 298 K; CO_2 loading 0 mol/mol).

side because of a very small mass transfer resistance in the gas phase to overall mass transfer resistance. Then, the CO_2 concentration starts to decline gradually in the membrane side due to a relatively high increase in the membrane resistance compared to corresponding values in the gas-phase. Additionally, the position of the gas-liquid contacting interface is determined by the membrane wetting ratio. From this Figure, the gas-liquid contacting interface is gradually shifted from the membrane surface to the membrane inside due to the penetration of more absorbents into membrane pores as membrane wetting ratio increases from 0% (non-wetted) to 100% (completely wetted).

Fig. 9 indicates the CO_2 concentration of gas-phase in the shell side along the membrane module with the membrane wetting from 0% (non-wetted) to 100% (completely wetted). Normally, the initial CO_2 concentration in the shell side decreases almost linearly from the top of the membrane module until it reaches its minimum in the bottom of the membrane module (gas outlets) as CO_2 is absorbed into DEAB solution continuously. As shown in Fig. 9, the CO_2 concentration of non-wetted is invariably lower compared to that of the wetted mode. This behavior can be attributed to the fact that membrane wetting causes the lower CO_2 sequestration from the gas phase and it means that the CO_2

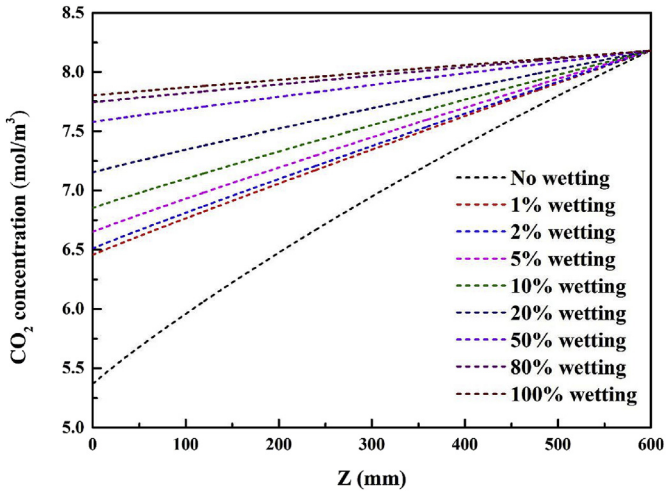

Fig. 9. The axial CO_2 concentration in the shell side along the membrane module. (DEAB 2 mol/L; CO_2 partial pressure 20 kPa; CO_2 Liquid velocity 0.012 m/s; Gas velocity 0.239 m/s; liquid feed temperature 298 K; CO_2 loading 0 mol/mol).

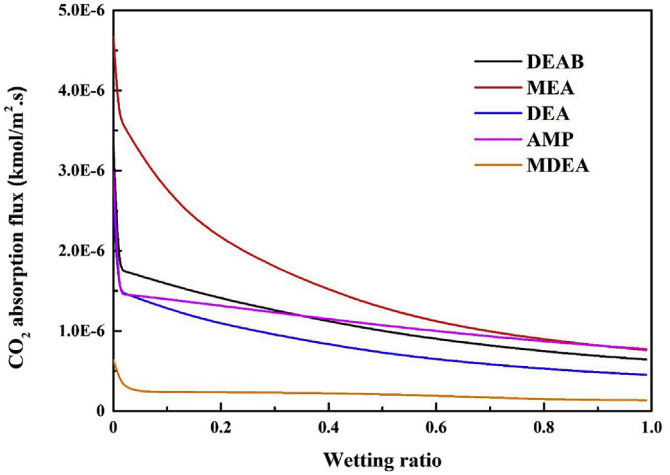

Fig. 10. The effect of wetting ratio on the CO_2 absorption flux (amine 2 mol/L; CO_2 partial pressure 20 kPa; Liquid velocity 0.042 m/s; Gas velocity 0.159 m/s; liquid feed temperature 298 K; CO_2 loading 0 mol/mol).

concentration in gas phase will be increased eventually.

There is no doubt that it is almost impossible to totally prevent membrane wetting in the process of CO_2 chemical absorption. The deterioration in the CO_2 absorption flux caused by membrane wetting was further investigated. As shown in Fig. 10, it is found that membrane wetting has a significantly adverse effect on the mass transfer performance of CO_2 absorption into different amine solutions even in the initial phase of membrane wetting, which causes the lower CO_2 separation from the gas phase. For DEAB, when the wetting ratio is just at a low extent (i.e. wetting ratio = 0.05), CO_2 absorption flux drops by up to 49.4% in comparison with that of a fresh membrane (non-wetted mode of operation). Similar observations were also reported by Zhang et al. [50]. In addition, the CO_2 absorption flux using AMP as absorbent is higher than that of DEAB and equal to that of MEA as wetting ratio increases from about 0.35 to 1 due to the higher reaction with CO_2 and higher CO_2 absorption capacity compared to DEAB and MEA, respectively.

3.3. Effects of operational conditions on enhancement factor and the overall gas-phase mass transfer coefficient

The effects of liquid velocity on the enhancement factors and the overall mass transfer coefficients of the non-wetted and partially-wetted modes as shown in Figs. 11a and 12a. It can be seen that the enhancement factor drops with liquid velocity. The reaction between CO_2 and DEAB solution can be assumed to occur in the intermediate fast-instantaneous regime (There is no obvious difference between *Ha* andE_∞) controlled by the combined effect of chemical reaction rate and mass transfer rate is at the whole liquid velocity range. At low liquid velocity of under 0.009 m/s, the section of intermediate regime has a certain characteristic of instantaneous regime (*Ha* is slightly larger than$E_\infty$and *E* is closer to E_∞ relative to *Ha*), which is mainly reflected in that the overall mass transfer coefficients are significantly affected by the liquid velocity because the overall mass transfer coefficient in the liquid phase with chemical reaction (Ek_L) increases with the liquid velocity proportionally. This phenomenon can be attributed to that the most chemical reactions tend to occur in an interface within the liquid film adjacent to gas-liquid contacting interface instead of the liquid bulk due to the high mass transfer resistance in the liquid phase. As liquid velocity increases continuously, the growth of the overall mass transfer coefficients starts to drop due to the decrease in the liquid phase mass transfer resistance. In this case, the significance of liquid phase mass transfer resistance is decreased as *Ha* decreases from 312 to 106 due to increase in $k_{L,ext}$ with liquid velocity and E_∞ increases from

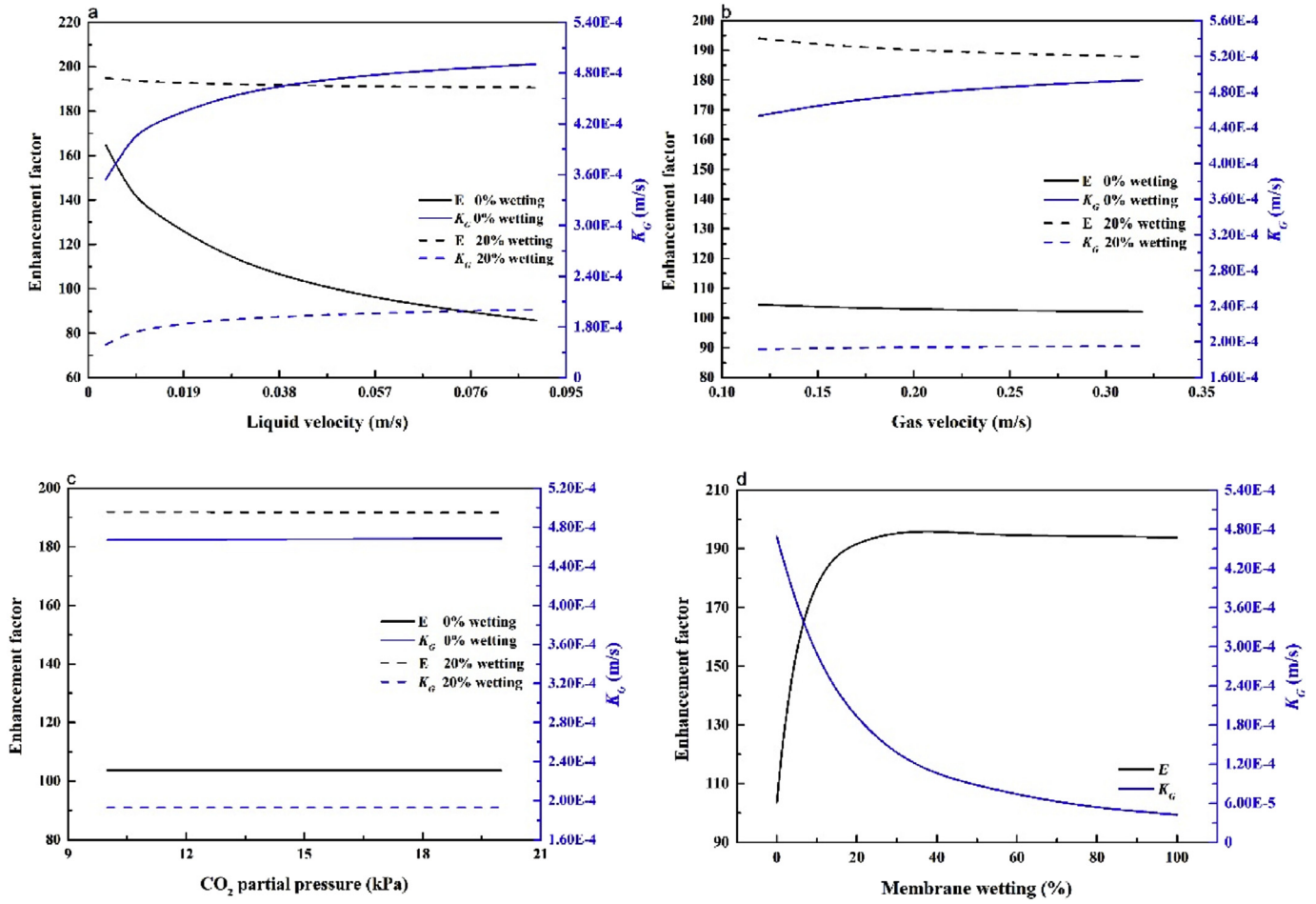

Fig. 11. The effect of operating parameters on the Enhancement factor and overall gas-phase mass transfer coefficient. (a) Liquid velocity; (b) Gas velocity; (c) CO_2 partial pressure; (d) Membrane wetting (amine 2 mol/L; temperature 298 K; CO_2 loading 0 mol/mol).

228 to 247, which indicates that the value of E_∞ has exceeded that of *Ha*, the enhancement factor approaches *Ha* at higher liquid velocities and the absorption regime has been transferred from the intermediate fast-instantaneous to the fast gradually. Also, the significance of liquid velocity in different CO_2 absorption regimes were reported by Dindore et al. [51], Rongwong, et al. [52]. Their simulated results revealed that liquid velocity has a more remarkable effect on CO_2 absorption flux in the instantaneous regime than the fast regime. As a contrast, the enhancement factor slightly decreases with liquid velocity for the partially-wetted compared to corresponding value of non-wetted mode with the reductions of 2.1% and 47.6%, respectively. Accordingly, the CO_2 absorption regime is regarded as the intermediate fast-instantaneous region that is extremely closer to instantaneous region at the whole liquid velocity range in consideration of interrelation of *E*, *Ha* andE_∞ (*Ha* is always much larger than E_∞ and *E* is closer to E_∞). Moreover, the overall mass transfer coefficient for the partially-wetted mode is affected less significantly by liquid velocity than the case for non-wetted mode with 26% and 38.4% rise, respectively. Since the fast-growing wetted membrane resistance starts to play a dominant role in contrast to the liquid phase resistance in mass transfer behavior of CO_2 absorption using membrane contactor.

From Fig. 11b, both the overall mass transfer coefficients of the non-wetted and partially-wetted mode slightly increases by 8.8% and 1,9%, respectively as gas velocity increases from 0.119 m/s to 0.319 m/s on account of the slight decrease in overall mass transfer resistance caused by smaller gas phase mass transfer resistance. However, the relatively low contribution of the gas phase mass transfer resistance to the overall mass transfer resistance for both of operating modes leads to a less noticeable enhancement in mass transfer performance by increasing gas velocity. For the non-wetted and partially-wetted modes, the chemical reaction between CO_2 and DEAB solution belongs to the intermediate fast-instantaneous region which are more likely to approach the fast regime ($E_\infty$is always larger than *Ha* and *E* is closer to *Ha*) and the instantaneous regime (*Ha* is always larger than$E_\infty$and *E* is closer toE_∞), respectively as shown in Fig. 12b. According to Eq (44), more supplement of CO_2 molecules with increasing gas velocity causes a higher concentration of CO_2 at the interface of the liquid phase and consequentlyE_∞decreases. Additionally, from Eq (42), *Ha* is constant due to its no direct relation with gas velocity. Hence, as seen from figure, in this region, the enhancement factors decrease with the reduction ofE_∞.

Moreover, as presented in Figs. 11c and 12c, it seems that CO_2 partial pressure has no significant effect on the enhancement factor and the overall mass transfer coefficients of the non-wetted and partially-wetted mode because *Ha* is unaffected by CO_2 partial pressure and the decrease in $E_\infty$is also extremely small due to the negligible increase in the concentration of CO_2 at the interface of the liquid phase, and the variation of CO_2 concentration in gas phase cause extreme small change in the overall mass transfer resistance at low CO_2 partial pressure range of 10 kPa–20 kPa, respectively.

Figs. 11d and 12d reveals that membrane wetting have an obvious influence on the enhancement factor and the overall mass transfer coefficients from 0% membrane wetting (non-wetted mode) to 100% membrane wetting (completely-wetted mode). At low membrane wetting (0–10%), the chemical reaction occurs intermediate fast-instantaneous regime closer to the fast regime. In this region, the enhancement factors are affected by *Ha* more thanE_∞. From Eq (42), the

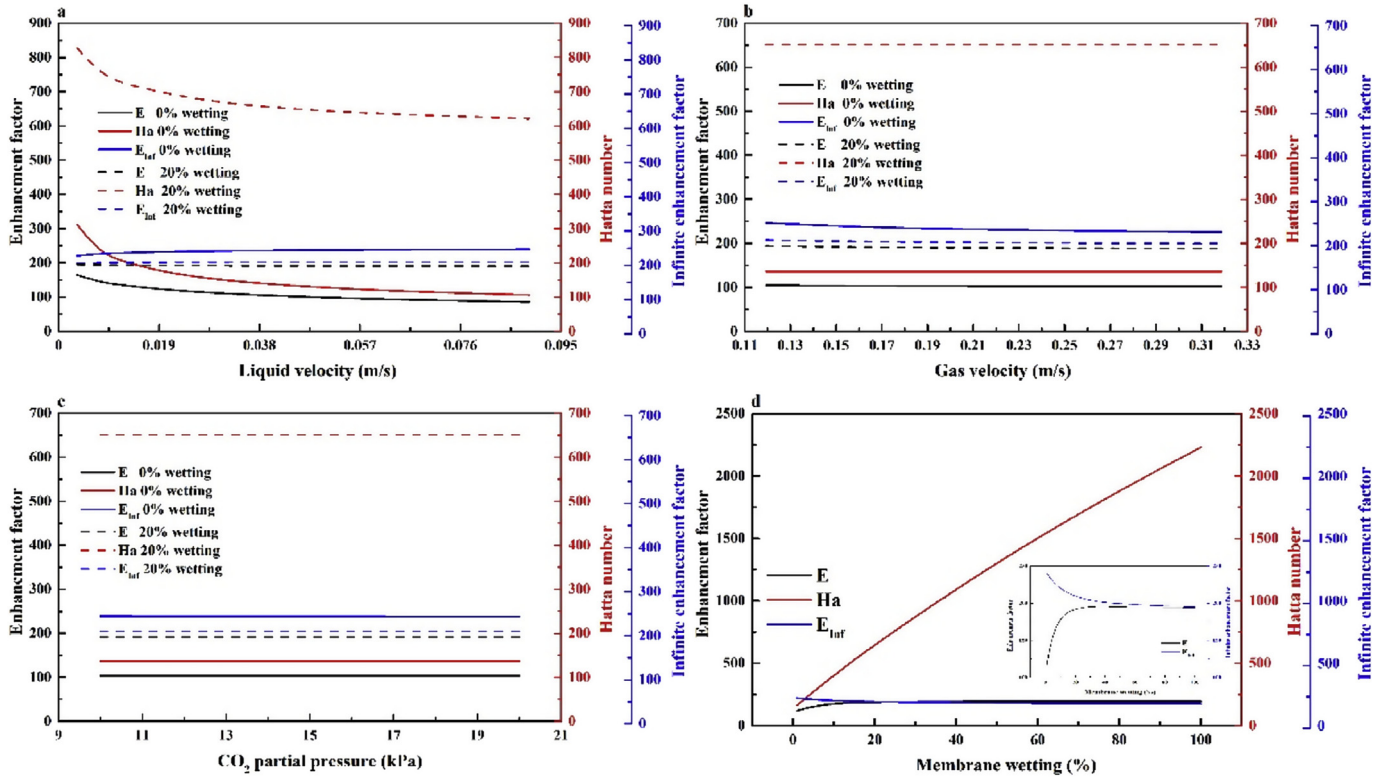

Fig. 12. The effect of operating parameters on the Enhancement factor, Infinite enhancement factor and Hatta number. (a) Liquid velocity; (b) Gas velocity; (c) CO_2 partial pressure; (d) Membrane wetting (amine 2 mol/L; temperature 298 K; CO_2 loading 0 mol/mol).

increase of wetted membrane resistance with membrane wetting is responsible for the decrease in item of $k_{L,ext}$, resulting in an increased *Ha*. Therefore, it can be observed that the enhancement factor rapidly increases from 103 to 178 as *Ha* increases. When membrane wetting increases to an intermediate level (10%–30%), the increase in enhancement factor begins to slow down (from 178 to 193) correlated with absorption regime completely into the intermediate fast-instantaneous to as significance of *Ha and*E_∞reduces and increases, respectively. Then, the enhancement factor has reached a peak (from 193 to 197) and appears a slowly decreasing trend and to be constant (from 197 to 195) at the membrane wetting range of 30%–100% as chemical reaction gradually occurs in the region transferred from the intermediate fast-instantaneous to the instantaneous (as$E_\infty$is decreased). Since shorter non-wetted membrane is achieved with membrane wetted, leading to less loss in the diffusion of CO_2 from the gas bulk, across the non-wetted membrane pores to the gas-liquid interface and obtaining a higher CO_2 concentration at the interface of the liquid phase. Especially, *Ha*, $E_\infty$and *E* are 2228, 194 and 195 for completely-wetted mode, respectively, which represents that *Ha* has been much larger than$E_\infty$and *E* is almost equal toE_∞within instantaneous regime. As for the overall mass transfer coefficient, it decreases by 80.3% with 50% membrane wetting, namely, from 4.68E-4 m/s to 8.77E-5 m/s due to dominance of wetted-membrane resistance in the overall mass transfer resistance. With the further increase of membrane wetting, the limited increase in proportion of wetted-membrane resistance causes less noticeable reduction in the overall mass transfer coefficient. It is reasonable to refresh the wetted membrane by blowing dry air or replace with new membrane when membrane wetting reaches 50%.

3.4. Mass transfer resistance analysis

The total mass transfer resistance of the non-wetted and the partially-wetted membrane contactor can be calculated by Eqs (16)–(18), respectively. In general, in the process of membrane CO_2 absorption, the mass transfer resistance of the gas phase makes negligible contribution, which can be attributed to the dominance of the mass transfer resistance of the liquid phase and membrane in the total mass transfer resistance [53,54]. The individual mass transfer resistances,R_L, R_m, $R'_m$and$R_G$were determined according to Eqs ((21), (29), (34) and (40), respectively. In addition, the calculations of the individual mass transfer resistance contribution of the liquid phase, the non-wetted membrane, the wetted membrane and the gas phase can be shown as R_L/R_{tot}, R_m/R_{tot}, R'_m/R_{tot}andR_G/R_{tot}, respectively. Fig. 13 indicates the contribution of the individual mass transfer resistance for the non-wetted mode and the partially wetted mode at various liquid velocities, gas velocities and CO_2 partial pressures. For the non-wetted mode (Figures a, c and e), the mass transfer resistance of the gas phase accounts for around 9.7–13.5%, 7.1–16.3% and around 13% whereas the proportions for the non-wetted membrane are 10.4%–14.4%, 13.3%–14.4% and around 13.5% at the whole range of liquid velocities, gas velocities and CO_2 partial pressures, respectively. In contrast, for the partially-wetted mode (20% wetting), the contribution of mass transfer resistance of the wetted-membrane increases rapidly from 57.1% to 73.6% with increasing liquid velocity. Also, the increase in related proportion is considered to be lower than that of case where wetting ratio increases with liquid velocity actually. Moreover, the wetted membrane resistances account for 69%–74% and around 70% in the overall mass transfer resistance with variation of gas velocity and CO_2 partial pressure, respectively. It can be concluded that the mass transfer resistance of wetted membrane phase has played a leading role in the overall mass transfer resistance compared to that of the liquid phase.

Furthermore, the effect of membrane wetting on individual mass transfer resistance was also discussed. As the liquid penetrates into the membrane pores, the membrane mass transfer resistance increases. From Fig. 14, the proportion of membrane mass transfer resistance shows a rapid increase from 13.7% to 75.3% at the low percent of membrane wetting range of 0–20%. At higher percent of membrane

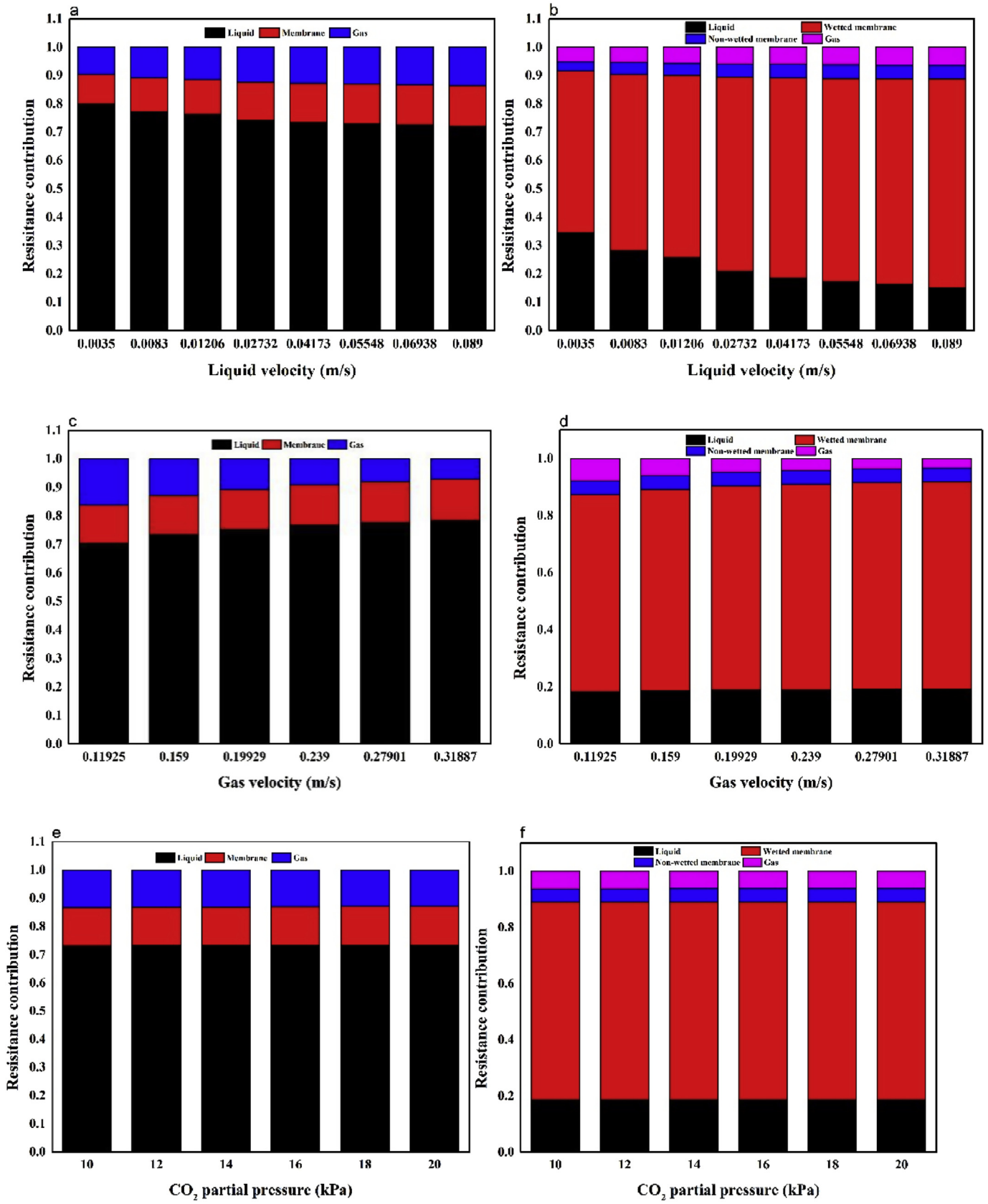

Fig. 13. The effect of operating parameters on contribution of individual resistance to overall resistance of the non-wetted mode and the partially wetted mode with 20% wetting. (a–b) Liquid velocity; (c–d) Gas velocity; (e–f) CO_2 partial pressure. (DEAB 2 mol/L; liquid feed temperature 298 K; CO_2 loading 0 mol/mol).

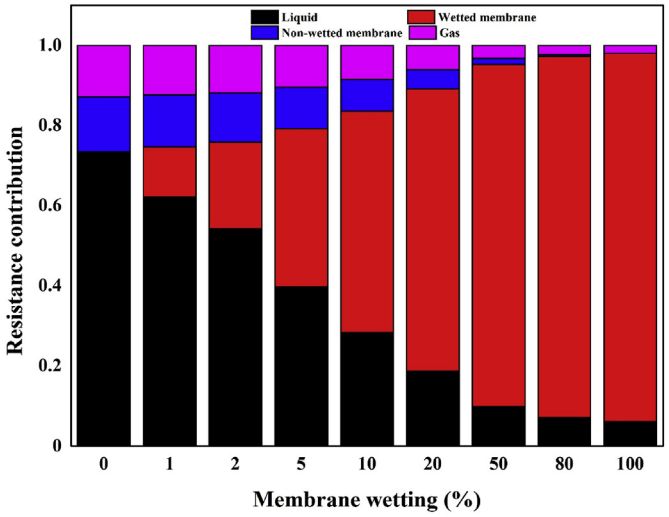

Fig. 14. The effect of membrane wetting on contribution of individual resistance to overall resistance (DEAB 2 mol/L; CO_2 partial pressure 20 kPa; Liquid velocity 0.042 m/s; Gas velocity 0.159 m/s; liquid feed temperature 298 K; CO_2 loading 0 mol/mol).

wetting, this change becomes less obvious with an only 16.6% increase from partially-wetted mode (20%) to completely-wetted mode (100%). It can be concluded that membrane mass transfer resistance, in the case of partially liquid-filled membrane pores, has a more significant influence on the CO_2 absorption performance at low percent of membrane wetting range. It must be emphasized that membrane wettability should be prevented to achieve the best performance of CO_2 capture in the membrane contactors. Researchers have proposed several approaches including membrane surface modification, application of a novel hydrophobic membrane, optimized operating conditions, and using absorbents with higher surface tension [55].

4. Conclusion

A 2-D mathematical model was conducted to investigate the mass transfer performance of CO_2 absorption into aqueous DEAB solution in a non-wetted and partially-wetted mode of HFMC in comparison with that of MEA, DEA, MDEA and AMP. The effects of operation parameters on the CO_2 absorption performance in HFMC including liquid and gas velocity and CO_2 partial pressure were systematically investigated. As a result, the simulated results reveal that the CO_2 absorption flux enhances with increasing liquid velocity and CO_2 partial pressure, and slightly increases with increasing gas velocity. Comparison of different amine solution reveals that the separation performance of DEAB is higher than that of DEA, MDEA and MEA and is also competitive with MEA. With wetting ratio increasing from 0% to 20%, the proportion of the membrane mass transfer resistance in the overall mass transfer resistance shows a rapid increase from 13.7% to 75.3%. The mass transfer in the region of wetted membrane has become the rate-controlling step compared to that in the liquid phase. CO_2 absorption performance and the overall mass transfer coefficient decreases by 49.4% and 80.5% when membrane wetting ratio are 5% and 50%, respectively, which reveals that CO_2 absorption performance will deteriorate with membrane wetting. Moreover, the CO_2 absorption flux and the overall mass transfer coefficient rapidly decreases as membrane wetting increases. The chemical reaction between CO_2 and DEAB for the non-wetted mode takes place in the intermediate fast-instantaneous regime, and it changes to the instantaneous regime when the membrane is partially wetted by analyzing the variation of enhancement factor.

Acknowledgments

The financial support from the National Natural Science Foundation of China (NSFC-Nos. 21536003, 21706057, 21878073 and 51521006), the Natural Science Foundation of Hunan Province in China (No. 2018JJ3033), and the China Outstanding Engineer Training Plan for Students of Chemical Engineering & Technology in Hunan University (MOE-No. 2011–40).

Appendix A. Supplementary data

Supplementary data to this article can be found online at https://doi.org/10.1016/j.memsci.2019.117439.

References

[1] Z. Liang, W. Rongwong, H. Liu, et al., Recent progress and new developments in post-combustion carbon-capture technology with amine based solvents, Int. J. Greenh. Gas Contr. 40 (2015) 26–54.
[2] G.T. Rochelle, Amine scrubbing for CO_2 capture, Science 325 (5984) (2009) 1652–1654.
[3] C. Zheng, D. Demontigny, Experimental study of carbon dioxide absorption into aqueous ammonia with a hollow fiber membrane contactor, J. Membr. Sci. 540 (2017) 297–306.
[4] S. Zhao, P.H.M. Feron, L. Deng, et al., Status and progress of membrane contactors in post-combustion carbon capture: a state-of-the-art review of new developments, J. Membr. Sci. 511 (2016) 180–206.
[5] A.K. Pabby, A.M. Sastre, State-of-the-art review on hollow fibre contactor technology and membrane-based extraction processes, J. Membr. Sci. 430 (3) (2013) 263–303.
[6] Z. Wang, M. Fang, H. Yu, et al., Experimental and modeling study of trace CO_2 removal in a hollow-fiber membrane contactor, using CO_2-loaded monoethanolamine, Ind. Eng. Chem. Res. 52 (50) (2013) 18059–18070.
[7] A. Comite, C. Costa, M. Demartini, et al., Rate of CO_2 transfer to loaded MEA solutions using a membrane contactor device, Int. J. Greenh. Gas Contr. 52 (2016) 378–386.
[8] I.M. Bernhardsen, H.K. Knuutila, A review of potential amine solvents for CO_2 absorption process: absorption capacity, cyclic capacity and pKa, Int. J. Greenh. Gas Contr. 61 (2017) 27–48.
[9] X. Luo, S. Liu, H. Gao, et al., An improved fast screening method for single and blended amine-based solvents for post-combustion CO_2 capture, Separ. Purif. Technol. 169 (2016) 279–288.
[10] M. Xiao, H. Liu, R. Idem, et al., A study of structure–activity relationships of commercial tertiary amines for post-combustion CO_2 capture, Appl. Energy 184 (2016) 219–229.
[11] F.A. Chowdhury, H. Yamada, Y. Matsuzaki, et al., Development of novel synthetic amine absorbents for CO_2 capture, Energy Procedia 63 (2014) 572–579.
[12] T. Sema, A. Naami, K. Fu, et al., Comprehensive mass transfer and reaction kinetics studies of a novel reactive 4-diethylamino-2-butanol solvent for capturing CO_2, Chem. Eng. Sci. 100 (2013) 183–194.
[13] T. Sema, M. Edali, A. Naami, et al., Solubility and diffusivity of N_2O in aqueous 4-(Diethylamino)-2-butanol solutions for use in postcombustion CO_2 capture, Ind. Eng. Chem. Res. 51 (2) (2012) 925–930.
[14] T. Sema, A. Naami, R. Idem, et al., Correlations for equilibrium solubility of carbon dioxide in aqueous 4-(Diethylamino)-2-butanol solutions, Ind. Eng. Chem. Res. 50 (24) (2011) 14008–14015.
[15] K. Maneeintr, R.O. Idem, P. Tontiwachwuthikul, et al., Synthesis, solubilities, and cyclic capacities of amino alcohols for CO_2 capture from flue gas streams, Energy Procedia 1 (1) (2009) 1327–1334.
[16] M. Saidi, Mathematical modeling of CO_2 absorption into novel reactive DEAB solution in hollow fiber membrane contactors; kinetic and mass transfer investigation, J. Membr. Sci. 524 (2017) 186–196.
[17] S. Masoumi, P. Keshavarz, Z. Rastgoo, Theoretical investigation on CO_2 absorption into DEAB solution using hollow fiber membrane contactors, J. Nat. Gas Sci. Eng. 18 (2014) 23–30.
[18] M. Afkhamipour, M. Mofarahi, Modeling and optimization of CO_2 capture using 4-diethylamino-2-butanol (DEAB) solution, Int. J. Greenh. Gas Contr. 49 (2016) 24–33.
[19] A.T. Nakhjiri, A. Heydarinasab, O. Bakhtiari, et al., Experimental investigation and mathematical modeling of CO_2 sequestration from CO_2/CH_4 gaseous mixture using MEA and TEA aqueous absorbents through polypropylene hollow fiber membrane contactor, J. Membr. Sci. 565 (2018) 1–13.
[20] N. Goyal, S. Suman, S.K. Gupta, Mathematical modeling of CO_2 separation from gaseous-mixture using a Hollow-Fiber Membrane Module: physical mechanism and influence of partial-wetting, J. Membr. Sci. 474 (2015) 64–82.
[21] S. Boributh, W. Rongwong, S. Assabumrungrat, et al., Mathematical modeling and cascade design of hollow fiber membrane contactor for CO_2 absorption by monoethanolamine, J. Membr. Sci. 401–402 (2012) 175–189.
[22] M. Caplow, Kinetics of carbamate formation and breakdown, J. Am. Chem. Soc. 90 (24) (1968) 6795–6803.
[23] P.V. Danckwerts, The reaction of CO_2 with ethanolamines, Chem. Eng. Sci. 34 (4)

(1979) 443–446.
[24] R. Faiz, M. Al-Marzouqi, Mathematical modeling for the simultaneous absorption of CO_2 and H_2S using MEA in hollow fiber membrane contactors, J. Membr. Sci. 342 (1) (2009) 269–278.
[25] R.J. Littel, W.P.M.V. Swaaij, G.F. Versteeg, Kinetics of carbon dioxide with tertiary amines in aqueous solution, AIChE J. 36 (11) (1990) 1633–1640.
[26] C. Zheng, B. Zhao, K. Wang, et al., Determination of kinetics of CO_2 absorption in solutions of 2-amino-2-methyl-1-propanol using a microfluidic technique, AIChE J. 61 (12) (2015) 4358–4366.
[27] J. Günther, P. Schmitz, C. Albasi, et al., A numerical approach to study the impact of packing density on fluid flow distribution in hollow fiber module, J. Membr. Sci. 348 (1) (2010) 277–286.
[28] S. Atchariyawut, R. Jiraratananon, R. Wang, Mass transfer study and modeling of gas-liquid membrane contacting process by multistage cascade model for CO_2 absorption, Separ. Purif. Technol. 63 (1) (2008) 15–22.
[29] Z. Zhang, F. Chen, M. Rezakazemi, et al., Modeling of a CO_2-piperazine-membrane absorption system, Chem. Eng. Res. Des. 131 (2017) 375–384.
[30] M.C. Yang, E.L. Cussler, Designing hollow-fiber contactors, AIChE J. 32 (11) (1986) 1910–1916.
[31] R.C. Reid, J.M. Prausnitz, T.K. Sherwood, The Properties of Gases and Liquids, third ed. ed., McGraw-Hill, New York, 1977.
[32] F.M. Mourits, F.H.A. Rummens, A critical evaluation of Lennard–Jones and Stockmayer potential parameters and of some correlation methods, Can. J. Chem. 55 (16) (2011) 3007–3020.
[33] Z. Wang, M. Fang, S. Yan, et al., Optimization of blended amines for CO_2 absorption in a hollow-fiber membrane contactor, Ind. Eng. Chem. Res. 52 (34) (2013) 12170–12182.
[34] A.T. Nakhjiri, A. Heydarinasab, O. Bakhtiari, et al., The effect of membrane pores wettability on CO_2 removal from CO_2/CH_4 gaseous mixture using NaOH, MEA and TEA liquid absorbents in hollow fiber membrane contactor, Chin. J. Chem. Eng. 26 (2018) 1845–1861.
[35] J. Happel, Viscous flow relative to array of cylinders, AIChE J. 5 (2) (1959) 174–177.
[36] W.J. DeCoursey, Absorption with chemical reaction: development of a new relation for the Danckwerts model, Chem. Eng. Sci. 29 (9) (1974) 1867–1872.
[37] S. Khaisri, D. deMontigny, P. Tontiwachwuthikul, et al., A mathematical model for gas absorption membrane contactors that studies the effect of partially wetted membranes, J. Membr. Sci. 347 (1–2) (2010) 228–239.
[38] G.F. Versteeg, W.V. Swaalj, Solubility and diffusivity of acid gases (carbon dioxide, nitrous oxide) in aqueous alkanolamine solutions, J. Chem. Eng. Data 33 (1) (1988) 29–34.
[39] T. Sema, A. Naami, Z. Liang, et al., Analysis of reaction kinetics of CO_2 absorption into a novel reactive 4-diethylamino-2-butanol solvent, Chem. Eng. Sci. 81 (2012) 251–259.
[40] A. Aboudheir, P. Tontiwachwuthikul, A. Chakma, et al., Kinetics of the reactive absorption of carbon dioxide in high CO_2-loaded, concentrated aqueous monoethanolamine solutions, Chem. Eng. Sci. 58 (23–24) (2003) 5195–5210.
[41] X. Zhang, A. Chengfang Zhang, Y. Liu, Kinetics of absorption of CO_2 into aqueous solution of MDEA blended with DEA, Ind. Eng. Chem. Res. 41 (5) (2006) 1135–1141.
[42] E.R. Gilliland, Diffusion coefficients in gaseous systems, Ind. Eng. Chem. 26 (6) (1934) 681–685.
[43] J.J. Ko, T.C. Tsai, C.Y. Lin, et al., Diffusivity of nitrous oxide in aqueous alkanolamine solutions, J. Chem. Eng. Data 46 (1) (2001) 160–165.
[44] S.M. Melnikov, M. Stein, Molecular dynamics study of the solution structure, clustering, and diffusion of four aqueous alkanolamines, J. Phys. Chem. B 122 (10) (2018) 2769–2778.
[45] E.D. Snijder, M.J.M. te Riele, G.F. Versteeg, et al., Diffusion coefficients of several aqueous alkanolamine solutions, J. Chem. Eng. Data 38 (3) (1993) 475–480.
[46] L.C. Chang, A. Tongi Lin, M.H. Li, Mutual diffusion coefficients of some aqueous alkanolamines solutions, J. Chem. Eng. Data 50 (1) (2005) 77–84.
[47] A. Penttilä, C. Dell'Era, P. Uusi-Kyyny, et al., The Henry's law constant of N_2O and CO_2 in aqueous binary and ternary amine solutions (MEA, DEA, DIPA, MDEA, and AMP), Fluid Phase Equilib. 311 (2011) 59–66.
[48] W. Rongwong, C. Fan, Z. Liang, et al., Investigation of the effects of operating parameters on the local mass transfer coefficient and membrane wetting in a membrane gas absorption process, J. Membr. Sci. 490 (S1) (2015) 236–246.
[49] Z. Cui, D. Demontigny, Experimental study of carbon dioxide absorption into aqueous ammonia with a hollow fiber membrane contactor, J. Membr. Sci. 540 (15) (2017) 297–306.
[50] H.Y. Zhang, R. Wang, D.T. Liang, et al., Theoretical and experimental studies of membrane wetting in the membrane gas–liquid contacting process for CO_2 absorption, J. Membr. Sci. 308 (1–2) (2008) 162–170.
[51] V.Y. Dindore, D.W.F. Brilman, G.F. Versteeg, Hollow fiber membrane contactor as a gas–liquid model contactor, Chem. Eng. Sci. 60 (2) (2005) 467–479.
[52] W. Rongwong, S. Assabumrungrat, R. Jiraratananon, Rate based modeling for CO_2 absorption using monoethanolamine solution in a hollow fiber membrane contactor, J. Membr. Sci. 429 (2) (2013) 396–408.
[53] S. Boributh, S. Assabumrungrat, N. Laosiripojana, et al., Effect of membrane module arrangement of gas–liquid membrane contacting process on CO_2 absorption performance: a modeling study, J. Membr. Sci. 372 (1–2) (2011) 75–86.
[54] P. Jin, C. Huang, Y. Shen, et al., Simultaneous separation of H_2S and CO_2 from biogas by gas–liquid membrane contactor using single and mixed absorbents, Energy Fuels 31 (2017) 11117–11126.
[55] S. Mosadegh-Sedghi, D. Rodrigue, J. Brisson, et al., Wetting phenomenon in membrane contactors – causes and prevention, J. Membr. Sci. 452 (452) (2014) 332–353.